15R $SrMn_{1-x}Fe_xO_{3-\delta}$ ($x \approx 0.1$); A New Perovskite Stacking Sequence

Edmund J. Cussen,[†] Jeremy Sloan,[†,‡] Jaap F. Vente,[†] Peter D. Battle,*[,†] and Terence C. Gibb[§]

Inorganic Chemistry Laboratory, University of Oxford, South Parks Road, Oxford OX1 3QR, U.K., Department of Materials, University of Oxford, Parks Road, Oxford OX1 3QR, U.K., and School of Chemistry, Leeds University, Leeds LS2 9JT, U.K.

Received July 10, 1998

A polycrystalline sample of a new phase in the Sr−Fe−Mn−O system has been prepared by standard solid-state techniques. Characterization at room temperature by X-ray diffraction, high-resolution electron microscopy, Mössbauer spectroscopy and neutron diffraction has led to it being described as a 15-layered, rhombohedral (15R) perovskite [space group $R\bar{3}m$: $a = 5.4489(1)$ Å, $c = 33.8036(7)$ Å] with a previously unobserved structure. The pseudo close-packed SrO_3 layers have a $(cchch)_3$ stacking sequence such that the occupation of the interstitial 6-coordinate sites by Mn (or Fe) leads to the formation of Mn_2O_9 units which are linked to each other either directly by a common vertex, or indirectly via a single, vertex-sharing MnO_6 octahedron. The stoichiometry of the compound was determined to be $SrMn_{0.915(5)}Fe_{0.085(5)}O_{2.979(3)}$. The face-sharing sites are occupied by 0.957(3)Mn/0.043(3)Fe while the exclusively corner-linked sites show a higher Fe occupation; 0.745(4)Mn/0.255(4)Fe. A neutron diffraction experiment carried out at 3 K indicated the presence of long-range magnetic order with the Mn^{4+} cations aligned antiferromagnetically with an ordered moment of $2.26(3)\mu_B/Mn^{4+}$. Both the neutron and the susceptibility data are consistent with the Fe cations remaining magnetically disordered to 3 K. The latter data show $T_N = 220$ K, and suggest that some spin frustration is present at low temperatures.

Introduction

The crystal structures of perovskites, ABX_3, can be considered to consist of pseudo close-packed layers of stoichiometry AX_3 with the smaller cation, B, occupying the octahedral interstitial sites between layers. The stacking of the successive layers can be either cubic close-packed (ccp) or hexagonal close-packed (hcp), leading respectively to corner-sharing or face-sharing of adjacent BO_6 octahedra. The presence of only ccp leads to the well-known perovskite structure of $CaTiO_3$,[1] while only face-sharing octahedra are present in the purely hcp form of $BaNiO_3$,[2] designated 2H. The structure adopted by a particular compound is dependent on a number of factors including the electronic structure of the B cation, oxygen stoichiometry and the size ratio $r_a:r_b$.[3] As a result of this, compounds which might be expected to have the same structure can adopt very different crystal structures. For example, $SrFeO_3$[4] adopts a cubic perovskite structure containing only vertex-sharing FeO_6 octahedra whereas, at room temperature, $SrMnO_3$ has a 4H perovskite structure[5] made up of face-sharing Mn_2O_9 dimers linked to each other by vertexes. The stacking arrangement in the latter compound is neither pure ccp nor pure hcp, but a periodic sequence (*hchc*) of both. The large number of pressure and temperature-dependent phase transitions observed for several systems[6,7] indicates that the stability difference between different stacking sequences is often small. Furthermore, as there are many different possible stacking sequences containing various proportions of cubic and hexagonal stacking,[8] a compound of composition $AB_{1-x}B'_xO_3$ may adopt a structure which has a ratio of cubic:hexagonal stacking intermediate between those of ABO_3 and $AB'O_3$. We have previously demonstrated this to be the case at the composition $SrMn_{0.72}Fe_{0.28}O_{2.87}$, which adopts a 10H structure consisting of 80% cubic stacking.[9] The electronic properties of perovskites are dependent on the adopted structure, and an understanding of the structural chemistry of these phases is crucial if we are to develop novel structures showing useful magnetic properties. We can now report a structural and magnetic study of a compound of nominal composition $SrMn_{0.9}Fe_{0.1}O_3$ which has a stacking sequence never previously observed.

Experimental Section

The black polycrystalline sample of $SrMn_{0.9}Fe_{0.1}O_3$ was prepared by heating a well ground, pelleted, stoichiometric mixture of $SrCO_3$, MnO_2, and Fe_2O_3 in air at temperatures increasing to 1350 °C. This resulted in a single phase product having the well-known 6H perovskite structure.[10] This material was then annealed at 1200 °C for 5 weeks during which time a new phase formed. Subsequent treatment at 1300 °C followed by annealing for 3 days at 1200 °C (this cycle being repeated 4 times) resulted in complete conversion of the 6H perovskite into the new phase. The final heat treatment at 1200 °C was followed by air-quenching. The product was insoluble, and we were therefore unable to perform a volumetric analysis to determine the oxygen content. X-ray powder diffraction data were collected in the angular range $10° < 2\theta < 120°$ in steps of $\Delta 2\theta = 0.02°$ using a Siemens

[†] Inorganic Chemistry Laboratory, University of Oxford.
[‡] Department of Materials, University of Oxford.
[§] Leeds University.

(1) Kay, H. F.; Bailey, P. C. *Acta Crystallogr.* **1957**, *10*, 219.
(2) Lander, J. J. *Acta Crystallogr.* **1951**, *4*, 148.
(3) Goodenough, J. B.; Kafalas, J. A. *J. Solid State Chem.* **1973**, *6*, 493.
(4) MacChesney, J. B.; Sherwood, R. C.; Potter, J. F. *J. Chem. Phys.* **1965**, *43*, 1907.
(5) Battle, P. D.; Gibb, T. C.; Jones, C. W. *J. Solid State Chem.* **1988**, *74*, 60.
(6) Negas, T.; Roth, R. S. *J. Solid State Chem.* **1970**, *1*, 409.
(7) Negas, T.; Roth, R. S. *J. Solid State Chem.* **1971**, *3*, 1971.
(8) *International Tables for X-ray Crystallography*; The Kynoch Press: Birmingham, 1959; Vol. II, p 342.
(9) Battle, P. D.; Davison, C. M.; Gibb, T. C.; Vente, J. F. *J. Mater. Chem.* **1996**, *6(7)*, 1187.
(10) Lightfoot, P.; Battle, P. D. *J. Solid State Chem.* **1990**, *89*, 174.

10.1021/ic980802j CCC: $15.00
Published on Web 10/29/1998

Table 1. HRTEM Parameters for EMS Image Simulations

accelerating voltage	400 kV
spherical aberration coefficient (C_s)	0.9 nm
semi-convergence angle (α)	0.8 mrad
objective lens aperture diameter	10 nm^{-1}

D5000 diffractometer operating with Cu $K\alpha_1$ radiation in Bragg−Brentano geometry. Neutron powder diffraction data were collected in the angular range $10° < 2\theta < 140°$ in steps of 0.05°, $\lambda = 1.5938$ Å, on diffractometer D2b at the Institut Laue-Langevin in Grenoble at both room temperature and 3 K. The sample, ≈5.5 g, was contained in a 16 mm diameter vanadium can. All the diffraction data, uncorrected for absorption, were analyzed by profile analysis[11] using the GSAS[12] suite of programs. The background was fitted by a Chebyshev polynomial and the peak shape was described by a pseudo-Voigt function.

High-resolution electron microscopy (HREM) was performed on a JEOL 4000EX electron microscope operated at 400 kV. This microscope was fitted with a top-loading double-tilt goniometer specimen stage and was capable of a minimum point resolution of 1.6 Å. The specimens were prepared by ultrasonically dispersing the sample in chloroform, and then placing the dispersion dropwise onto a 3 mm 300 mesh lacy carbon coated copper grid. All images were recorded close to the optimum Scherzer defocus conditions. HREM multislice image simulations were carried out with the EMS suite of image simulation programs,[13] using the microscope parameters listed in Table 1. The image simulations were computed using the lattice parameters and refined atomic coordinates obtained from the simultaneous refinement of room-temperature X-ray and neutron diffraction data.

Magnetic measurements were performed using a Quantum Design SQUID magnetometer. The susceptibilities were recorded in fields of 100 and 1000 G after cooling in both zero field and the measuring field. Hysteresis measurements were carried out at 5 and 250 K in fields between 10^4 and -10^4 G after the sample had cooled in a field of 10^4G.

Mössbauer spectra were collected at room temperature using a ^{57}Co/Rh source matrix, also held at room temperature. Isomer shifts were calibrated relative to metallic iron.

Results

Initial heating of the metal oxides at temperatures below 1350 °C resulted in a mixture of 4H and 6H perovskites. Although the Mn/Fe distribution between the 4H and 6H phases could not be determined by X-ray diffraction, attempts to synthesize Fe-doped 4H $SrMnO_3$ have indicated that the solubility limit of Fe in the 4H structure is in the range 3−5 mol % $SrFeO_3$ in $SrMnO_3$ and is largely temperature independent.[14] The formation of the 6H/4H mixture therefore results in segregation into regions which are either significantly Fe-rich or Fe-deficient relative to the bulk sample. Heating at 1350 °C was necessary to form a single phase (6H) of the desired composition. Upon subsequent heating at lower temperatures sharp peaks indicative of the formation of a new phase appeared in the diffraction pattern. The new peaks increased in intensity while the $l \neq 0$ reflections of the 6H material decreased. The modified pattern included peaks of similar intensity to, and at approximately the same angles as, the {*hk*0} reflections observed in the 4H and 6H materials indicating that the new phase was also a perovskite with $a \approx 5.45$ Å. The remaining reflections could be indexed with $c \approx 33.8$ Å indicative of a 15-layer unit cell. There are only two stacking sequences which can result in a unit cell of this size and these can be described in terms of mixed stacking of hexagonal (*h*) and cubic (*c*) layers of SrO_3 leading to rhombohedral unit cells. One of these sequences, $(hhhhc)_3$, has been reported in $BaMnO_{3-\delta}$.[6] From the intensity distribution in our diffraction data it was clear that our sample is not isostructural with this phase. However, the data could readily be fitted utilizing the space group $R\bar{3}m$ and three crystallographically distinct sites for each of Sr, Mn/Fe, and O with the atomic positions based on the stacking of the SrO_3 layers in a $(cchch)_3$ sequence. As can be seen in Figure 1, this stacking sequence results in three distinct octahedral interstitial sites; two are linked by a common face to give dimers similar to those seen in 4H $SrMnO_3$ while the third is linked exclusively by corner-sharing as in $SrFeO_3$. X-ray diffraction is insensitive to Fe/Mn ordering over these sites and so the data were refined simply using the scattering factor of Mn to describe the transition metal distribution. The eight atomic coordinates, two lattice parameters, and three isotropic temperature factors associated with the structure were refined. Temperature factors of atoms of the same type were constrained to be the same and fractional occupancies of the oxygen sites were not refined. The refined instrumental parameters were one scale factor, seven background parameters, four profile parameters and one zero point. A full refinement of these parameters resulted in the following residuals: $R_{wp} = 5.08$, $R_p = 3.98$, $R_I = 10.74$, $\chi^2_{red} = 1.638$, DWd = 1.320 (lower limit of 90% confidence level = 1.925).[15]

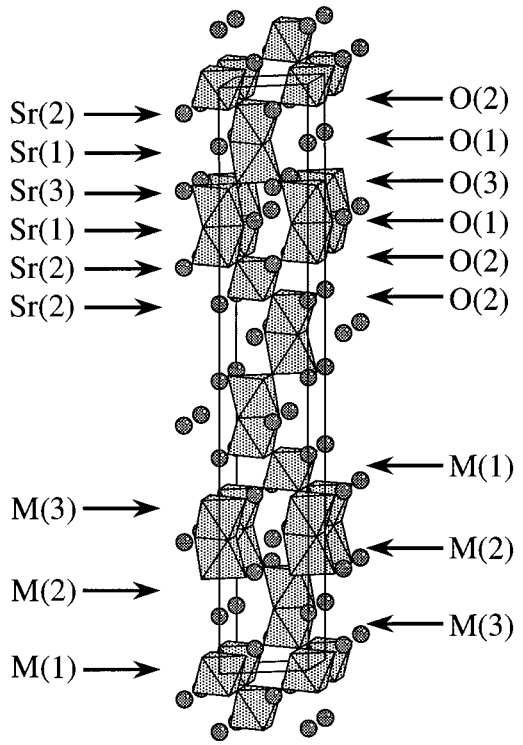

Figure 1. 15R crystal structure of perovskite ABO_3: circles represent A cations, octahedra represent BO_6 units. The three transition metal sites are labeled.

Electron micrographs and selected area electron diffraction (ED) patterns obtained parallel to the [0 $\bar{1}$ 0] zone axis were used to confirm the stacking sequence and to test the extent of ordering of the 15R phase. Figure 2 shows an indexed electron diffraction pattern corresponding to the [0 $\bar{1}$ 0] zone axis, the corresponding lattice image of the crystal and a simulated image calculated from the refined structure using a defocus of 75 nm and a crystal thickness of 2.2 nm. Figure 2 clearly shows that

(11) Rietveld, H. M. *J. Appl. Crystallogr.* **1969**, *2*, 65.
(12) Larson, A. C.; von-Dreele, R. B. *General Structure Analysis System (GSAS)*; Report LAUR 86-748; Los Alamos National Laboratories: Los Alamos, NM, 1990.
(13) Stadelmann, P. A. *Ultramicroscopy* **1987**, *21*, 131.
(14) Cussen, E. J. Unpublished results.
(15) Hill, R. J.; Flack, H. D. *J. Appl. Crystallogr.* **1987**, *20*, 356.

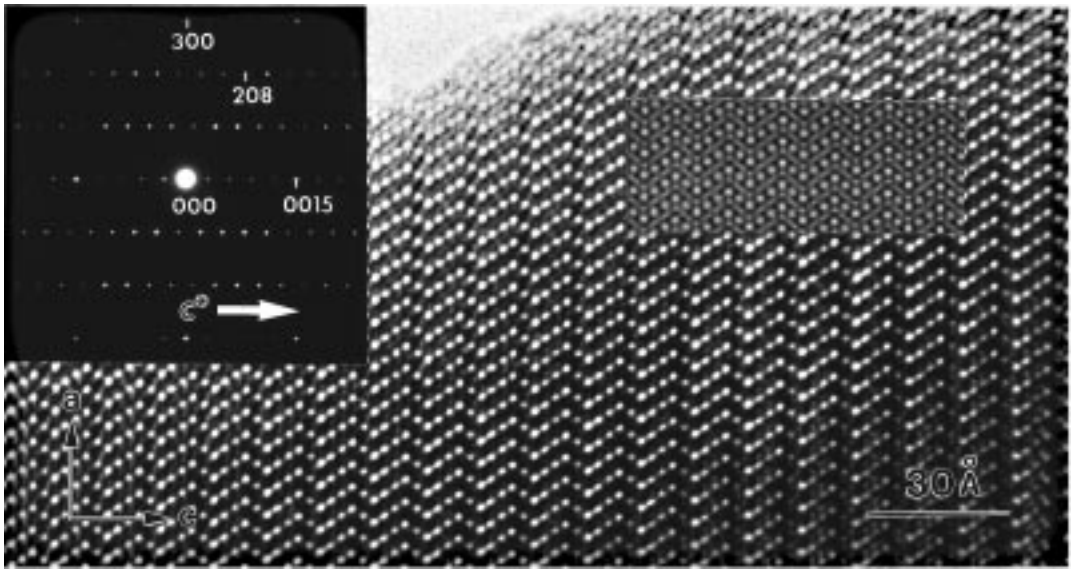

Figure 2. Electron diffraction pattern of 15R $SrMn_{1-x}Fe_xO_{3-\delta}$ ($x \approx 0.1$) indexed as the [0 $\bar{1}$ 0] zone axis, the corresponding lattice image, and the simulated image based on the refined structure.

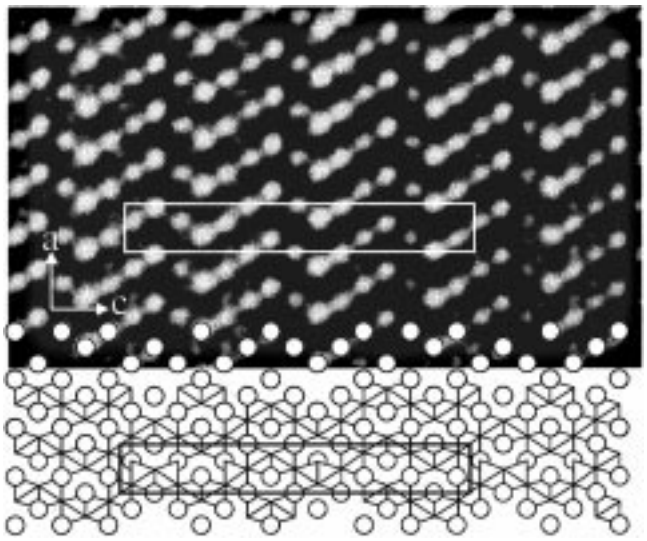

Figure 3. Imaged and refined crystal structure of 15R $SrMn_{1-x}Fe_xO_{3-\delta}$ ($x \approx 0.1$) viewed along [0 $\bar{1}$ 0]. The unit cell is outlined in both cases.

the ordering of the stepped structure extends over at least 200 Å. The 15 SrO_3 layers which constitute a unit cell span three of the lamellae, each ≈11 Å wide, which are apparent in the micrograph. The rising zigzag motif of white dots, which repeats with a period of ≈33.7 Å, allows us to identify the *c* parameter of the unit cell. Figure 3 shows the close correspondence between the observed lattice image and the structure derived from the X-ray diffraction experiment; the white dots clearly correspond to Sr^{2+} cations. Twenty-two fragments were identified with the same zone axis and, of these, only one fragment showed any sign of disorder as a result of planar faults, caused by intergrowth with other polytypes.

In the absence of an iodometric analysis, we relied on Mössbauer spectroscopy for an estimate of the Fe^{3+}/Fe^{4+} ratio, and hence the oxide vacancy concentration, in our sample. The spectrum collected at room temperature is shown in Figure 4. The resonance is comparatively broad, with evidence of considerable unresolved structure. Such a broadening is not uncommon in iron oxides which exhibit local disorder; the isomer shift of iron does change significantly if the number of coordinated oxide ions changes and although cation disorder

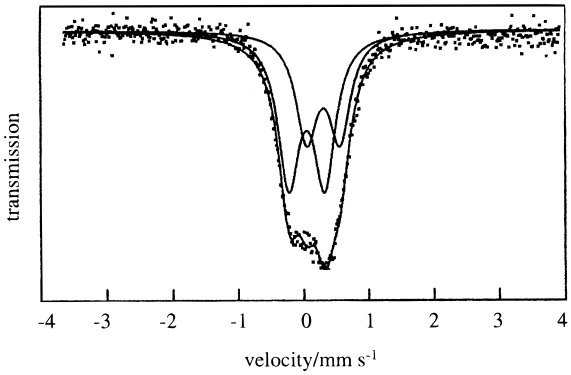

Figure 4. Observed and fitted Mössbauer spectrum of 15R $SrMn_{1-x}Fe_xO_{3-\delta}$ ($x \approx 0.1$) at room temperature.

in the second coordination sphere has only a small effect on the isomer shift, it can result in significant changes in the quadrupole splitting at individual sites. Consideration of available data on Sr/Fe perovskite phases,[5,9,16,17] shows that Fe^{3+} in 6-coordination to oxygen has an isomer shift of ∼0.37 mm s^{-1}, while Fe^{3+} in 4-coordination gives a value of ∼0.17 mm s^{-1}. Five-coordination is rare in these phases, but it is reasonable to assume that the isomer shift would fall between these values, and that a value of ∼0.27 mm s^{-1} might be expected. The isomer shift for high-spin Fe^{4+} is not well defined as few compounds are known and some of these have a measure of metallic character or disproportionate to Fe^{3+}/Fe^{5+}. The phase Sr_2FeO_4 shows an isomer shift of −0.01 mm s^{-1} at room temperature,[17] and the value computed for ^{57}Fe-doped $SrMnO_3$ [5] is also −0.01 mm s^{-1}; we shall take this as a representative figure in the present discussion. The data in Figure 4 are sufficiently complex that we are unable to provide a unique description of the valence states and coordination numbers in the 15R sample. However, all our attempted fits suggested an Fe^{3+}/Fe^{4+} ratio of 1:1, within experimental error, with the majority of the reduced cations having a coordination number of less than 6. From the Fe^{3+}/Fe^{4+} ratio, and assuming Mn/Fe = 9:1, we can estimate the stoichiometry of our sample to be

(16) Battle, P. D.; Gibb, T. C. *J. Chem. Soc., Dalton Trans.* **1987**, 667.
(17) Dann, S. E.; Weller, M. T.; Currie, D. B.; Thomas, M. F.; Alrawwas, A. D. *J. Mater. Chem.* **1993**, *3*, 1231.

Table 2. Atomic Coordinates of 15R $SrMn_{1-x}Fe_xO_{3-\delta}$ ($x \approx 0.1$)[a] at Room Temperature from Combined Refinement of X-ray and Neutron Data

atom	*x*	*y*	*z*	$U_{11,22}$/Å^2	U_{33}/Å^2	U_{12}/Å^2	$U_{13,-23}$/Å^2
Sr(1)	0	0	0.09931(9)	0.0064(5)[b]			
Sr(2)	0	0	0.36860(9)	0.0078(6)[b]			
Sr(3)	0	0	$^1/_2$	0.0094(9)[b]			
Mn/Fe(1)	0	0	0	0.003(4)[b]			
Mn/Fe(2)	0	0	0.1971(2)	0.011(1)[b]			
Mn/Fe(3)	0	0	0.2715(1)	0.002(1)[b]			
O(1)	0.5127(2)	0.4873(2)	0.09965(5)	0.0108(6)	0.00949(7)	0.0082(8)	0.0009(4)
O(2)	0.5005(2)	0.4995(2)	0.36604(5)	0.0100(5)	0.0149(6)	0.0035(9)	0.0044(6)
O(3)	$^1/_2$	$^1/_2$	$^1/_2$	0.0095(8)	0.0162(9)	0.003(1)	−0.0043(7)

[a] Transition metal site occupations: M(1), 0.745(4)Mn/0.255(4)Fe; M(2) and M(3), 0.957(3)Mn/0.043(3)Fe. Space group $R\bar{3}m$; $a = 5.4489(1)$ Å, $c = 33.8036(7)$ Å, $V = 869.19(5)$ Å^3. [b] Isotropic temperature factor.

$SrMn_{0.9}Fe_{0.1}O_{2.975(2)}$, that is, more than 99% of the anion sites are occupied. Figure 4 shows the fit to two equal-area broad doublets with quadrupole splittings of 0.55 and 0.52 mm s^{-1} and isomer shifts of 0.028 and 0.28 mm s^{-1}; in a simplistic interpretation these two components can be assigned to 6-coordinate Fe^{4+} and 5-coordinate Fe^{3+}, respectively.

Unfortunately it was not possible to perform the neutron diffraction experiments until eight months after the initial X-ray data were collected. Prior to the neutron work a second set of X-ray diffraction data was collected and refined as above to give essentially the same quality of fit. However the peaks had broadened by ca. 20% indicating a reduction in the crystallinity of the sample. No peaks corresponding to a second phase were observed. This second data set still gave a good quality fit and heating the sample for 24 h at 1200 °C resulted in sharpened peaks with widths comparable to those observed from the freshly prepared sample. The neutron diffraction data were analyzed using the model described above but this analysis revealed extra intensity which could not be accounted for by a 15R model. As there was no apparent broadening of peaks at high angle it was decided that a second phase rather than a reduction in symmetry was responsible for this additional intensity and, indeed, the pattern could be satisfactorily fitted in a simultaneous refinement with the more recent X-ray data using a mixture of 98.0(3)% 15R and 2.0(3)% 4H $SrMnO_3$. The lattice parameters and atomic parameters of the second phase were set at the values obtained by Battle *et al.*[5] and were not refined, but preferred orientation was utilized to describe the intensity distribution resulting from this phase existing as a precipitate in the 15R matrix. The refinements of the principal phase initially included variable oxygen occupancy and three Mn/Fe site fractions. However, the fractional occupancies of the oxygen sites refined to unity and were subsequently set at this value and not refined. The Fe/Mn ratios on the M(2) and M(3) sites refined to be the same, within standard deviations, and so were constrained to be the same. The final refined metal occupancies of the face-sharing octahedral sites, M(2) and M(3), were 0.957(3)Mn/0.043(3)Fe, the M(1) sites showed a higher Fe occupancy, 0.745(4)Mn/0.255(4)Fe, giving a composition for the 15R phase $SrMn_{0.915(5)}Fe_{0.085(5)}O_3$, consistent with the target composition. The final atomic parameters are given in Table 2, and the most important bond distances and angles are presented in Table 3. The concentration of Fe on the face-sharing sites is in excellent agreement with the experimentally determined maximum solubility of Fe in 4H $SrMnO_3$. In total 61 variables were refined: 2 lattice parameters, 2 scale factors, 2 counter zero points, 1 phase fraction, 1 neutron wavelength, 16 background, 8 profile parameters (constrained to be the same for both phases in each histogram), 8 atomic positions, 6 metal isotropic temperature parameters, 9 oxygen anisotropic temperature factors, 2 Mn/Fe fractions, and 1 preferred orientation parameter. Introducing anisotropic thermal parameters at the cation sites produced no significant improvement in fit quality. The final fit has the agreement factors: $R_{wp} = 7.49$, $R_p = 5.46$, DWd = 0.349(<1.947), $R_I = 5.95$ for the neutron data, shown in Figure 5a, and $R_{wp} = 6.21$, $R_p = 4.95$, DWd = 1.609(<1.947), $R_I = 11.28$ for the X-ray data, shown in Figure 5b, with a combined $\chi^2_{red} = 3.074$.

Table 3. Selected Bond Lengths (Å) and Angles (deg) of 15R $SrMn_{1-x}Fe_xO_{3-\delta}$ ($x \approx 0.1$) at Room Temperature from Combined Refinement of X-ray and Neutron Data

Sr(1)−O(1)	2.7271(1) × 6	Mn(1)−O(2)	1.918(2) × 6
Sr(1)−O(2)	2.743(3) × 3	Mn(2)−O(1)	1.907(4) × 3
Sr(1)−O(3)	2.767(2) × 3	Mn(2)−O(3)	1.880(3) × 3
Sr(2)−O(1)	2.757(3) × 3	Mn(3)−O(1)	1.934(3) × 3
Sr(2)−O(2)	2.7258(2) × 6	Mn(3)−O(2)	1.860(3) × 3
Sr(2)−O(2)	2.787(2) × 3	Mn(2)−Mn(3)	2.513(5)
Sr(3)−O(1)	2.828(2) × 6	Mn(1)−Mn(3)	3.777(2)
Sr(3)−O(3)	2.72446(6) × 6	Mn(2)−Mn(2)	3.760(6)
shortest	O−O distance	O(1)−O(1)	2.516(3)

O(2)−Mn(1)−O(2)	90.11(9)	O(1)−Mn(3)−O(1)	81.1(2)
O(1)−Mn(2)−O(1)	82.5(2)	O(1)−Mn(3)−O(2)	91.79(6)
O(1)−Mn(2)−O(3)	92.08(4)	O(2)−Mn(3)−O(2)	94.5(2)
Mn(2)−O(1)−Mn(3)	81.7(1)	Mn(1)−O(2)−Mn(3)	176.8(2)

In addition to the crystallographic peaks observed at room temperature, the data collected at 3 K included peaks at low angles which could not be indexed in the crystallographic unit cell. The absence of any extra peaks at high angle indicated that these are due to magnetic ordering. They could be accounted for using a magnetic model which assumes that interactions between nearest neighbors are antiferromagnetic, resulting in a structure consisting of ferromagnetic sheets stacked antiferromagnetically along the *c* axis. The magnetic unit cell, a portion of which is shown in Figure 6, thus has dimensions $a \times a \times 2c$ relative to the chemical cell. After a number of trial refinements, the magnetic moments were constrained to align along the *x*-axis and the analysis of the low temperature neutron diffraction data was carried out as described above, but with the phase fractions and the Mn/Fe fractional occupancies constrained to the values obtained from the analysis of the room temperature data. Initially each transition metal site was assigned an independent magnetic moment, but this resulted in values which were equal when corrected for the manganese occupation. It is therefore tempting to assume that only Mn takes part in the long-range magnetic ordering and that no ordered magnetic contribution is observed from Fe cations. The final refinement was carried out with the magnetic moment of all Mn cations constrained to be equal and the moment of Fe set to zero. The Mn moment refined to a value of 2.26(3) μ_B. The final fit is shown in Figure 7 and has parameters $R_{wp} = 7.99$, $R_p = 5.99$, DWd = 0.350(<1.947), $R_I = 4.12$, and $\chi^2_{red} =$

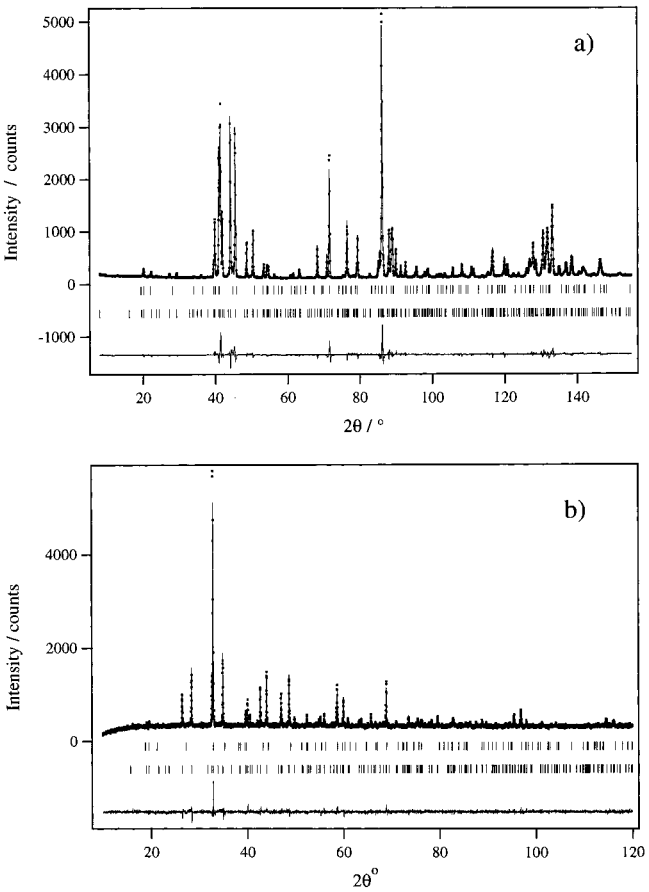

Figure 5. Observed (dots), calculated (full line), and difference neutron (a) and X-ray (b) powder diffraction patterns at 290 K. Reflection positions are indicated for 15R $SrMn_{1-x}Fe_xO_{3-\delta}$ ($x \approx 0.1$) (lower tick marks) and 2% $SrMnO_3$ (upper tick marks).

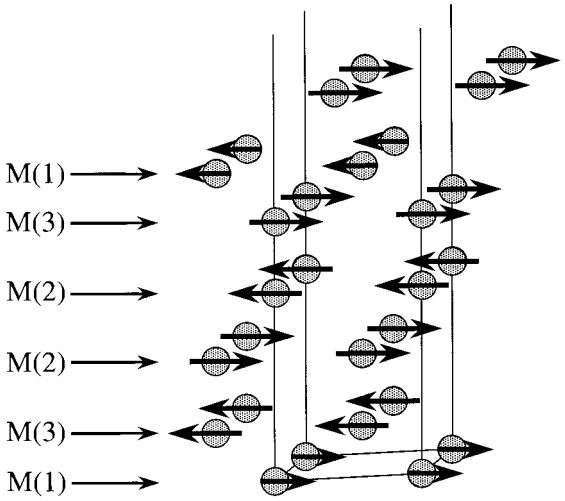

Figure 6. Antiferromagnetic ordering observed in 15R $SrMn_{1-x}Fe_xO_{3-\delta}$ ($x \approx 0.1$). Only magnetic ions are shown. The sites showing a reduced ordered moment associated with higher Fe occupation are indicated by a shortened arrow.

6.523 for 47 variables. The refined atomic parameters are shown in Table 4.

The magnetic susceptibility of the 15R product, measured in 100 G, is shown in Figure 8. In the temperature range $250 < T < 300$ K, the susceptibility was independent of field and could be fitted to a Curie−Weiss law, as shown, giving values of $\theta = -80$ K and $C = 1.25$ cm^3 K mol^{-1}, the latter value corresponding to $\mu_{eff} = 3.16\mu_B$ per transition metal. Only one

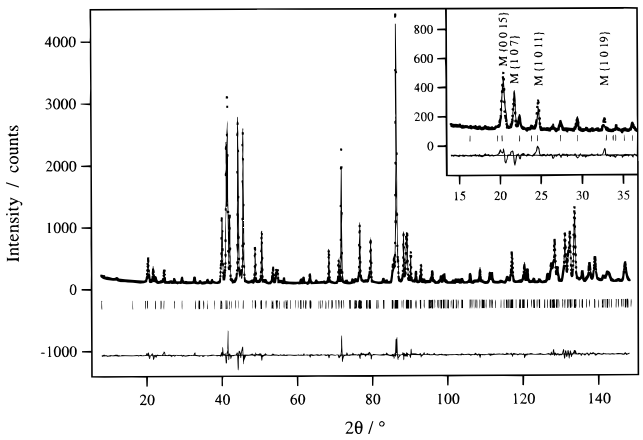

Figure 7. Observed (dots), calculated (full line) and difference neutron powder diffraction patterns of 15R $SrMn_{1-x}Fe_xO_{3-\delta}$ ($x \approx 0.1$) at 3 K. Nuclear reflections of the 15R phase are indicated by tick marks, inset shows indexing in the magnetic unit cell of the most intense magnetic reflections.

magnetic transition, at $T = 220$ K, is evident in the measured temperature range. Below this temperature there is divergence between the field cooled (FC) and zero field cooled (ZFC) data but the susceptibility continues to increase. The data in the range $10 < T < 220$ K could not be fitted by a Curie−Weiss law and the susceptibility showed a weak field dependence consistent with partial saturation. The variation of magnetization with field is shown in Figure 9. The measurement carried out at 250 K confirms that the sample is paramagnetic at this temperature. At 5 K a displaced hysteresis loop is observed. This is inconsistent with the simple idea of antiferromagnetic ordering developed above, and suggests the presence of frustrated spins in a more complex magnetic system.

Discussion

The formation of a single phase of nominal composition $SrMn_{1-x}Fe_xO_3$ ($x = 0.1$) at a temperature less than 1350 °C was not expected when this study began. Preliminary work had shown there to be a solubility gap at 1200 °C between the 4H structure formed by $SrMnO_3$ ($x = 0$) and the 6H structure adopted at low temperatures for $x > 0.2$. From this it was thought that the thermodynamic product of heating an $x \approx 0.9$ mixture in air at $T < 1350$ °C would be a mixture of Mn-rich 4H and Fe-rich 6H perovskites. The transformation of 6H to 15R on annealing at 1200 °C indicates that the latter is thermodynamically stable with respect to segregation into a 4H/6H mixture; the formation of the mixture during initial heating is presumably due to kinetic factors. The preparation of a sample by transformation of a higher temperature phase is an unusual procedure and gives us insight into the relative stabilities of these structures. As noted above, the rapid formation of the 4H/6H mixture at low temperatures causes a compositional segregation in the sample and the bulk stoichiometry is not achieved on a microscopic scale at temperatures less than 1350 °C, when a single 6H phase is formed. It is this segregation which necessitates the effective use of a single phase starting material of composition $SrMn_{0.9}Fe_{0.1}O_3$ rather than the individual metal oxides.

The 15R stacking sequence is intermediate between the 4H and 6H structures in its fraction of cubic/hexagonal stacking, and both the 4H and 6H stacking motifs can be seen in the unit cell. The fundamental 5-layer (*cchch*) building block of the 15R structure (Figure 1) can be considered to be derived from the 4H (*chch*) perovskite by insertion of one additional cubic

Table 4. Atomic Coordinates of 15R $SrMn_{1-x}Fe_xO_{3-\delta}$ ($x \approx 0.1$)[a] at 3 K from Refinement of Neutron Data

atom	x	y	z	$U_{11,22}$/Å^2	U_{33}/Å^2	U_{12}/Å^2	$U_{13,-23}$/Å^2
Sr(1)	0	0	0.0994(2)	0.0053(9)[b]			
Sr(2)	0	0	0.3688(2)	0.0053(9)[b]			
Sr(3)	0	0	1/2	0.011(2)[b]			
Mn/Fe(1)	0	0	0	0.00(1)[b]			
Mn/Fe(2)	0	0	0.1967(3)	0.006(1)[b]			
Mn/Fe(3)	0	0	0.2708(2)	−0.003(1)[b]			
O(1)	0.5120(3)	0.4881(3)	0.09947(7)	0.0094(9)	0.010(1)	0.008(1)	0.0000(7)
O(2)	0.5008(3)	0.4992(3)	0.36595(8)	0.0078(8)	0.014(9)	0.003(1)	0.0015(8)
O(3)	1/2	1/2	1/2	0.019(1)	0.009(1)	0.0096(2)	−0.002(1)

[a] Space group $R\bar{3}m$; $a = 5.43826(5)$ Å, $c = 33.7533(4)$ Å, $V = 864.50(2)$ Å^3. [b] Isotropic temperature factor.

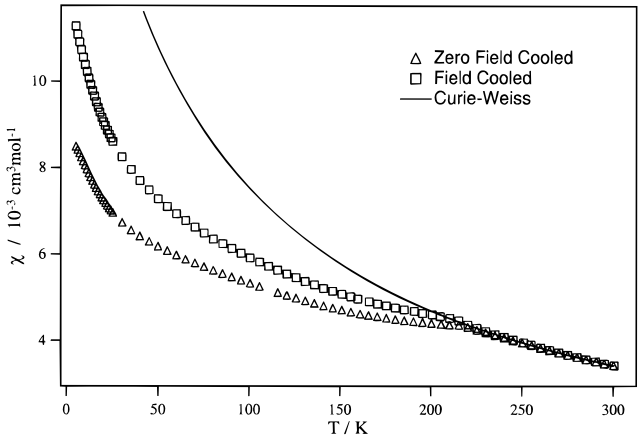

Figure 8. Molar magnetic susceptibility of 15R $SrMn_{1-x}Fe_xO_{3-\delta}$ ($x \approx 0.1$) as a function of temperature in 100 G. The data are fitted to a Curie−Weiss law in the range $250 < T < 300$ K.

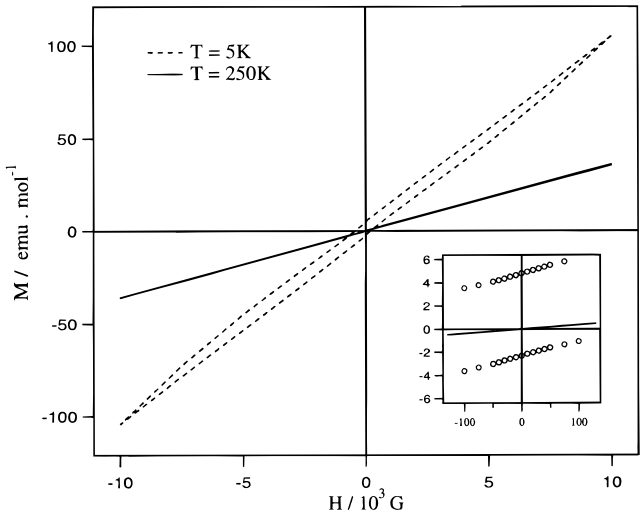

Figure 9. Magnetization of 15R $SrMn_{1-x}Fe_xO_{3-\delta}$ ($x \approx 0.1$) against applied field, measured at 250 and 5 K. Inset shows data around the origin.

layer into the four-layer unit cell. Similarly, it can be derived from the 6H (*cchcch*) structure by the removal of a single cubic layer. While it may be relatively simple to predict which regions of a phase diagram may show new stacking sequences and to estimate the ratio of cubic/hexagonal stacking, it is considerably more difficult to predict exact structures. The observation of this 15-layered perovskite demonstrates the point. A naïve model from which to predict structures in the Sr−Mn−Fe−O system might assume that face-sharing sites are occupied exclusively by Mn and that any Fe doped into the material will occupy corner-sharing sites. On this basis, substitution of 10% Fe for Mn on the interstitial sites should lead to a structure in which ≈10% of interstitial sites are exclusively corner linked, yet 20% of the sites in the 15R structure are so linked. It should be noted that the Mn occupancy of the corner-linked octahedral site, M(1) (74.5(4)%), is considerably greater than that observed in a similar site in the 10H $SrMn_{0.73}Fe_{0.27}O_{2.87}$ which showed ca. 55%. The 10H material was prepared by slow cooling, rather than air quenching as in the synthesis of 15R, and this suggests that the occupancy of M(1) by Mn in the 15R material deviates substantially from the low-temperature equilibrium value.

The concentration of anion vacancies in the 15R phase is too small to be detected by neutron diffraction, but our Mössbauer data show that approximately half of the Fe cations are in the trivalent state. If we use the Mn:Fe ratio determined in our neutron data analysis, and the Fe^{3+}/Fe^{4+} ratio of 1:1 estimated by Mössbauer spectroscopy, we conclude that the formula $SrMn_{0.915(5)}Fe_{0.085(5)}O_{2.979(3)}$ is the best representation of the 15R phase. This assumes that all Mn is in the +4 oxidation state. Given that the majority of the Fe lies on the corner-sharing M(1) site, it is reasonable to expect the highest vacancy concentration to occur on site O(2), but our neutron data do not allow confirmation of this hypothesis.

The bond lengths extracted from the 15R refinement are in good agreement with those found in previous studies of related compounds. As is expected, the M(1)−O(2) distance is intermediate between those found in the cubic perovskites $SrFeO_3$[4] and $SrMnO_3$.[6] The metal−oxygen distances in the dimers take a range of values due to the lower symmetry of the sites. 4H $SrMnO_3$, 4H $Ba_{0.1}Sr_{0.9}MnO_{2.96}$,[18] and 10H $SrMn_{0.73}Fe_{0.27}O_{2.87}$ show shorter distances from the metal to the corner-sharing oxygen atoms than to the face-sharing atoms, and analysis of the 15R data gives similar results for the M(2) and M(3) sites. The transition metal cations are displaced from the centers of the octahedra so as to increase the metal−metal separation in the dimers (to 2.513(5) Å), thus reducing the electrostatic repulsion between like ions. The shortest oxygen−oxygen distance found in the 15R material is that between the oxygen atoms in the shared face of the octahedra. The positioning of the oxygen atoms close to one another in the shared face further minimizes the repulsion between the cations, and is a common feature of face-sharing dimers. The refinement of the data collected at 3K did not reveal any unusual changes in bond lengths on cooling from room temperature and the reduction in unit cell volume, 0.54(4)%, is isotropic within the precision of our measurements.

The insensitivity of X-ray diffraction to the small amount of 4H phase observed in the neutron diffraction measurement makes it difficult to speculate about its origin. Electron microscopy is a poor technique for detecting such small quantities and it is unlikely that the small number of crystallites studied would include any of the 2% impurity. It is possible

(18) Jacobson, A. J.; Horrox, A. J. W. *Acta Crystallogr.* **1976**, *B32*, 1003.

that the 4H phase was present, but undetected, in the 6H intermediate, or alternatively it could be associated with the reduction in crystallinity over time, which was recognized by peak broadening in the X-ray pattern. The difference in M(1) Mn occupancies in the air-quenched 15R material and the slow-cooled 10H suggest that for the composition $SrMn_{0.915}Fe_{0.085}O_3$, the 15R structure is not the equilibrium phase at room temperature. It is possible that the observed peak broadening is associated with the very slow transformation of $SrMn_{0.915}Fe_{0.085}O_3$ to $SrMnO_3$ and an Fe-rich 15R phase with a Mn occupancy of the M(1) site reduced toward the value observed in the 10H material. It is also possible that the deterioration of the sample was due to subtle changes in the oxygen content.

The value of the paramagnetic moment above 220K, $\mu_{eff} = 3.16\ \mu_B$ per transition metal, is low compared to the spin only value 4.00 μ_B expected for composition $SrMn_{0.915(5)}Fe_{0.085(5)}O_{2.979(3)}$. However this is in keeping with a previous study of 4H $SrMnO_3$.[5] In the 4H material, antiferromagnetic coupling between Mn^{4+} cations in the face-sharing octahedral sites takes place at ca. 350 K leading to a reduction in the observed paramagnetic moment above the Néel temperature of 278 K. The face-sharing octahedral sites in the 15R material have 95.7(3)% Mn occupancy and a Mn−Mn separation of 2.513(5) Å (cf. 2.500(6) Å in $SrMnO_3$) and it therefore seems likely that the reduced paramagnetic moment observed in the range $245 < T < 300$ K is due to coupling in these face-sharing dimers. The coupling within the dimers is considerably stronger than between corner-linked octahedral sites and the latter do not couple until lower temperatures. We believe that the magnetic transition at 220 K represents the formation of a long-range magnetically ordered structure involving M(1), M(2) and M(3), and that the hysteresis below this temperature is due to partial magnetic frustration in the material. The origin of this frustration is not obvious, but it is possible that it is associated with the occupation of B sites by nonmagnetically ordered Fe ions. The magnetic structure adopted is such that the antiferromagnetic interactions between all neighboring Mn^{4+} cations are satisfied. The frustration may arise from next nearest neighbor (NNN) interactions which, although weaker than nearest neighbor (NN) interactions, can still determine the magnetic structure if they are sufficiently numerous.[19] The absence of a magnetically ordered cation in the NN M(1) sites adjacent to a Mn(3) cation may allow the sum of NNN interactions to dominate over the single remaining interaction with NN Mn(2). If, as expected, the NNN interaction is antiferromagnetic this would lead to spin frustration and hence give rise to the observed hysteresis effects. The low ordered magnetic moment per Mn^{4+} at 3 K, 2.26(3) μ_B, compared to the value predicted after allowing for a degree of covalency,[20] ca. 2.6 μ_B, also suggests a degree of magnetic frustration with apparently only ca. 80% of Mn^{4+} ions ordering at 3 K. While this low value could be attributed to other effects, for example, imperfect spin alignment beyond the resolution of our data or reduced antiferromagnetic domain size, the displacement of the hysteresis plot at 5 K suggests that the low ordered moment is, at least in part, due to spin frustration.

The apparent lack of magnetic order among the Fe cations is unexpected, but consistent with both the neutron diffraction data and the continued increase in the magnetic susceptibility below the Néel temperature. The Fe concentration at the M(2) and M(3) sites, 4.3(3)%, has a low impact on their average magnetic moment, but the 25.5(4)% occupancy of the M(1) sites by Fe results in a clear reduction in the observed ordered magnetic moment on this site. Consideration of the ≈180° superexchange between high-spin Fe^{3+} (d^5) or Fe^{4+} (d^4) and Mn^{4+} (d^3) via a bridging oxygen ion suggests that competing interactions will be present.[21] Superexchange between the metal e_g orbitals via the oxygen p_z would be ferromagnetic but the π interaction between the metal t_{2g} orbitals via oxygen p_x and p_y orbitals is antiferromagnetic. It should be noted that the symmetry of the M(1) site is such that whether the sign of the Fe−O−Mn exchange is positive or negative it can be accommodated into the long-range magnetic structure; the M(3) ions in the neighboring layers remain ferromagnetically aligned to one another. Given that ordered ferromagnetic alignment between Fe at M(1) and Mn^{4+} at M(3) would manifest itself as a reduced moment per Mn^{4+} at the M(1) position, the fact that we observe the same moment per Mn at M(1), M(2), and M(3) suggests that M(1) Fe is not involved in long-range magnetic order. It is possible that each M(1) Fe is experiencing a net exchange interaction close to zero, or that the range of environments causes these Fe spins to freeze in random directions, the number of static spins increasing with decreasing temperature. The nonfrozen spins are likely to be responsible for the increase in the magnetic susceptibility below T_N and the frozen spins are an alternative source of the observed hysteresis. The superexchange occurring between M(1) and neighboring M(3) Mn^{4+} is further complicated by oxide vacancies around Fe^{3+} cations and by Fe^{4+} having the electronic configuration $t_{2g}^3e_g^1$ and therefore being susceptible to a Jahn−Teller distortion. This was not observed in the refinement of the neutron diffraction data, cooperative ordering not being possible due to the low concentration of Fe^{4+} ions in the structure. The Jahn−Teller distortion would lead to a lengthening of bonds along one axis and a shortening along the others, or vice versa, with increased orbital overlap, and increasing exchange parameter, in the direction of shortened bonds while the interaction in the direction of lengthened bonds would be weakened. We believe that these local effects may be responsible for Fe remaining magnetically disordered at 3K in a lattice of ordered spins. A future low-temperature study by Mössbauer spectroscopy may clarify some of these issues.

In conclusion, we have been able to prepare the first example of a (cchch) 15R perovskite by taking care to avoid segregation into phases of different composition during synthesis. The success of our synthesis has been demonstrated by a combination of X-ray, neutron and electron diffraction. The material has been shown to order antiferromagnetically below 220 K, although the presence of Fe^{3+}, Fe^{4+} and Mn^{4+} leads to complex magnetic behavior.

Acknowledgment. We are grateful to EPSRC for financial support and to P. G. Radaelli for experimental assistance at ILL, Grenoble.

IC980802J

(19) Cussen, E. J.; Vente, J. F.; Battle, P. D.; Gibb, T. C. *J. Mater. Chem.* **1997**, *7*(3), 459.
(20) Tofield, B. C.; Fender, B. E. F. *J. Phys. Chem. Solids* **1970**, *31*, 2741.
(21) Goodenough, J. B. *Magnetism and the Chemical Bond*; Interscience: New York, 1963.